# Ground state of the two-dimensional electron gas

B. Tanatar and D. M. Ceperley
*National Center for Supercomputing Applications, University of Illinois at Urbana-Champaign, 605 East Springfield Avenue, Urbana, Illinois 61820*
*and Department of Physics, University of Illinois at Urbana-Champaign, 1110 West Green Street, Urbana, Illinois 61801*
(Received 7 November 1988)

Variational and fixed-node Green's-function Monte Carlo calculations have been performed to find the ground-state properties of the two-dimensional electron gas in the density range $1 \leq r_s \leq 100$. Our calculations predict a Wigner crystallization at the density $r_s \simeq 37 \pm 5$. The electron system is found to be in the normal- (paramagnetic) fluid state below the transition density, but the fully polarized state is very close in energy. We have tabulated the values of pair distribution function $g(r)$, the static structure factor $S(k)$, and the momentum distribution $n(k)$ at several densities of interest both in the normal and the polarized phases. An estimate of the spin susceptibility $\chi$ is also given.

## I. INTRODUCTION

The two-dimensional (2D) electron gas is both a fundamental model in many-body physics and has several important applications. First, the electronic motion in the copper-oxide planes are suggested to explain the high-transition-temperature superconductivity in new classes of superconducting materials. Secondly, the experimental study of the pure 2D electron gas is realized either by trapping electrons on the surface of liquid helium or more recently by trapping them on a film which is on a solid dielectric material.[1] Although in the former group of experiments the densities and temperatures have not been such as to study the quantum regime, it is possible that the quantum regime may be reached in the latter type of experiments. Finally, localized 2D electron states exist at the interface between GaAs and $Ga_{1-x}Al_xAs$ or at the interface of a metal oxide and a semiconductor [a metal-oxide-semiconductor (MOS) structure].[2] Such interfaces constitute important electronic devices and in a strong magnetic field display the integer and fractional quantum Hall effect.

Therefore, it is valuable both from theoretical and experimental standpoints to predict the properties and phases of an electron system for a complete range of densities and temperatures. This paper is concerned only with the zero-temperature properties of the electron gas. The ground-state properties of the 2D electron gas have been studied under various approximations such as the random-phase approximation (RPA), summation of ladder diagrams, and coupled-cluster method by several authors.[3–12] One of us has performed variational Monte Carlo (VMC) calculations to determine the energy of correlated wave functions. There also was a path-integral Monte Carlo calculation of the high-temperature crystallization density of the 2D electron gas.[13]

In this paper we report the results of more accurate variational (VMC) and fixed-node Green's-function Monte Carlo (FN-GFMC) calculations of the ground-state properties of the 2D electron gas in the liquid and solid phases. More specifically, we calculate the ground-state energy for the normal and fully-spin-polarized liquid phases and for the crystal phase. This enables us to determine the density at which the electron gas becomes a Wigner crystal, the energy versus density, the compressibility, and estimates of the magnetic susceptibility. We also calculate the radial distribution function, the static structure factor, and momentum distribution of the various phases of the electron gas.

The electron gas is a system of charged spin-$\frac{1}{2}$ fermions interacting with a Coulomb $(1/r)$ potential to which a uniform background is added for charge neutrality. The system at $T=0$ is characterized only by the dimensionless density parameter $r_s = a/a_0$, which is defined in terms of Bohr radius $a_0 = \hbar^2/me^2$ and the radius of the circle that encloses one particle on the average $a = 1/\sqrt{\pi\rho}$ and $\rho$ is the number density. At small $r_s$ (i.e., high density), the electrons form a weakly coupled Fermi liquid, while at large $r_s$ they undergo a phase transition and crystallize. Energies in this paper are in units of rydbergs/electron, 1 Ry $\equiv me^4/2\hbar^2$, while lengths are in units of $a$. The Hamiltonian of the interacting system of $N$ electrons in these units is

$$H = \frac{1}{r_s^2} \sum_{1 \leq i \leq N} \nabla_i^2 + \frac{2}{r_s} \sum_{1 \leq i < j \leq N} \frac{1}{|\mathbf{r}_i - \mathbf{r}_j|} + \text{const} . \quad (1)$$

## II. METHODOLOGY

The basic idea of a VMC simulation is that in order to estimate the ground-state average of any observable (most notably the ground-state energy), assuming a trial wave function with the correct symmetry $\psi_T(R)$, one samples the configurations drawn from the probability density function,

$$|\psi_T(R)|^2 \Big/ \int dR |\psi_T(R)|^2 , \quad (2)$$

 

in which $R$ stands for the $2N$ particle coordinates and is called a configuration. The Metropolis algorithm[14] is then used to carry out the sampling of this distribution. The estimate of the energy is an upper bound to the exact ground-state energy and, as will be shown, a good bound.

The second and more accurate method that is used to calculate ground-state properties is the fixed-node GFMC method. The Schrödinger equation is solved by treating it as a diffusion equation.[15] First, the Schrödinger equation is written in imaginary time, and multiplied by a trial function,

$$\frac{\partial f(R,t)}{\partial t}=\sum_{i=1}^{N}\frac{\hbar^2}{2m}\nabla_i(\nabla_i f-f\nabla_i \ln\psi^2) -(\psi^{-1}H\psi-E_T)f \ , \tag{3}$$

where $E_T$ is the trial energy. In the GFMC algorithm $f(R,t)$ is interpreted as the probability distribution in configuration space, and an initial ensemble of configurations with probability density $|\psi_T(R)|^2$ is evolved forward in time. When the convergence is reached at sufficiently large $t$, the probability distribution of points in the ensemble is given by $\phi(R)\psi_T(R)$ and it is called the *mixed distribution*. Here, $\phi(R)$ is an eigenvalue of the Hamiltonian with the fixed-node boundary conditions, $\phi(R)=0$ when $\psi_T(R)=0$. The fixed-node approximation is made to avoid the negative weights that would be otherwise generated by antisymmetric states. The fixed-node energy is an upper bound to the exact energy, but usually lies well below the variational energy. In calculations of the 3D electron gas we have found the fixed-node energy to be an extremely good upper bound.[8] Full discussion of these methods is found elsewhere.[8,16–18]

The form we choose for the trial wave function, a Slater-Jastrow or pair-product function, has been previously[6,8] used for the two- and three-dimensional electron gas and found to be accurate,

$$\psi_T(R)=D(R)\exp\left[-\sum_{1\le i<j\le N}u(|\mathbf{r}_i-\mathbf{r}_j|)\right] . \tag{4}$$

Here, $D(R)$ is the Slater determinant of single-body orbitals which antisymmetrizes the trial wave function. There are two separate determinates for the spin-up and spin-down electrons, and the polarization parameter is defined as $\xi=(N_\uparrow-N_\downarrow)/N$. In a liquid phase the orbitals are chosen to be the set of plane waves with wave vectors less than or equal to the Fermi wave vector for a given spin state.

The *pseudopotential* $u(r)$ correlates the electrons. We use the pseudopotential that minimizes the variational energy in the RPA as first derived by Gaskell.[19] In Ref. 6 this was shown to give lower energies than the parametrized Yukawa forms. Note that we are not making the RPA in evaluating the energy, but possibly taking a nonoptimal form for $u$ which will only affect the statistical error of the energy in a GFMC calculation since the nodes of the trial function are unaffected by the pseudopotential. This pseudopotential for a liquid reads

$$2u_{\rm RPA}(k)=-\frac{1}{S_0(k)}+\left[\frac{1}{S_0(k)^2}+\frac{4v(k)m}{\hbar^2k^2}\right]^{1/2} , \tag{5}$$

where $v(k)=2\pi e^2/k$ is the Fourier transform of the Coulomb potential, $S_0(k)$ is the static structure factor for the system of noninteracting fermions,

$$S_0(k)=\frac{2}{\pi}[\sin^{-1}y+y(1-y^2)^{1/2}] , \tag{6}$$

$y=k/2k_F$, and the Fermi wave vector is $k_F=\sqrt{2}$ (in the unpolarized case) in these units. The above pseudopotential $u$ possess properties which the optimal pseudopotential has, such as the cusp condition,

$$\lim_{r\to 0}\left[\frac{du(r)}{dr}\right]=-r_s , \tag{7}$$

and the long-range form necessary to have the correct plasmon dispersion,

$$\lim_{r\to\infty}[u(r)]=1.48\left[\frac{r_s}{r}\right]^{1/2} . \tag{8}$$

In the crystal phase the orbitals in the Slater determinant $D(R)$ are chosen to localize the electrons on the lattice sites. The centers of the orbitals $Z_k$ are a two-dimensional hexagonal lattice which has the lowest Madelung energy for 2D charged particles. The single-particle orbitals are chosen to be Gaussians, $\phi(r)=\exp[-C(r-Z_k)^2]$, where the $Z_k$ are a set of lattice sites, and the crystal pseudopotential is

$$2u(k)=-1-\frac{4C}{k^2}+\left[1+\frac{8C}{k^2}+\frac{4mv(k)}{\hbar^2k^2}\right]^{1/2} . \tag{9}$$

The width of the Gaussian orbitals $C$ is a density-dependent variational parameter previously[6] optimized. Two-dimensional crystals at finite temperatures will always have defects which destroy the long-range translational order; however, we expect that a two-dimensional crystal in the ground state will be free of defects. This assumption could be checked by either GFMC calculations at zero temperatures of path-integral Monte Carlo calculations at finite temperatures.

## III. SIZE DEPENDENCE

The energy of delocalized fermions depend very strongly on the number of particles or, equivalently, the size of the simulation cell. We must correct for this dependence in order to extrapolate to the thermodynamic limit. Ewald sums and periodic boundary conditions are used to eliminate the largest surface effects. However, substantial size effects remain. In the liquid phase we employ an extrapolation scheme based on the Fermi-liquid theory. According to Landau,[20] the energy of a system can be written as an energy functional of occupation numbers of quasiparticles, which behave just like an ideal Fermi gas. For small excitations from the ground state the functional can be linearized and is characterized by a few Fermi-liquid parameters. Consider how the energy of such an ideal Fermi-liquid changes when one goes from a finite system in periodic boundary conditions to an infinite system. For a finite system the allowed values of momentum lie on a lattice reciprocal to that of the simulation cell

TABLE I. Size dependence in the VMC method of normal electron fluid at $1 \le r_s \le 50$ and $\chi^2$-fit parameters. Also shown are the GFMC energy and the correlation energy $E_c(r_s,0)$. $\Delta$ is the difference between the fixed-node energy and the variational energy. Numbers in parentheses are the estimated errors (one standard deviation) in the last decimal place.

| | $r_s=1.0$ | $r_s=5.0$ | $r_s=10.0$ | $r_s=20.0$ | $r_s=30.0$ | $r_s=50.0$ |
|---|---|---|---|---|---|---|
| $N=26$ | −0.370(1) | −0.2937(1) | −0.168 66(5) | −0.091 73(2) | −0.063 31(2) | −0.039 318(8) |
| $N=42$ | −0.4451(7) | −0.2960(1) | −0.168 99(5) | −0.091 76(2) | −0.063 35(1) | −0.039 308(6) |
| $N=58$ | −0.3905(3) | −0.2940(3) | −0.168 51(5) | −0.091 65(4) | −0.063 309(6) | −0.039 301(5) |
| $N=74$ | −0.4156(8) | −0.2947(1) | −0.168 58(4) | −0.091 69(1) | −0.063 324(8) | −0.039 301(5) |
| $N=114$ | −0.3965(8) | −0.2937(1) | −0.168 46(3) | −0.091 65(1) | −0.063 293(8) | −0.039 296(4) |
| $E_\infty^{\mathrm{VMC}}$ | −0.4008(8) | −0.2936(1) | −0.168 34(4) | −0.091 62(1) | −0.063 291(1) | −0.039 290(5) |
| $b_1(r_s,0)$ | 1.11(1) | 0.041(2) | 0.007(1) | 0.0013(3) | 0.0007(2) | 0.000 03(1) |
| $b_2(r_s,0)$ | −0.41(4) | −0.047(5) | −0.016(2) | −0.0042(7) | −0.0015(6) | −0.0007(2) |
| $\chi^2$ | 6.4 | 2.4 | 1.3 | 0.2 | 1.7 | 0.1 |
| $E_{58}^{\mathrm{GFMC}}$ | −0.4092(6) | −0.2998(1) | −0.171 05(8) | −0.092 73(2) | −0.063 934(7) | −0.039 525(6) |
| $E_\infty^{\mathrm{GFMC}}$ | −0.420(1) | −0.2996(1) | −0.170 89(9) | −0.092 68(2) | −0.063 92(1) | −0.039 512(8) |
| $10^3\Delta_{\mathrm{MC}}$ | 19.2 | 6.0 | 2.56 | 1.06 | 0.63 | 0.22 |
| $E_c(r_s,0)$ | −0.217(1) | −0.0955(1) | −0.060 85(9) | −0.035 16(2) | −0.025 02(1) | −0.015 904(8) |

and the ground state is obtained by filling successive *shells* of these lattice points. (A shell consists of all lattice points related to each other by symmetry.) In the liquid phase, the number of electrons is chosen so that a shell is always filled. Then the only Fermi-liquid parameter which should enter is the effective mass. This implies that the size corrections of the interacting system should be proportional to the size correction of the noninteracting system, at least for large enough systems. The difference in energy per electron between an infinite and a finite ideal Fermi gas of $N$ electrons in periodic boundary conditions is of order $1/N$, with a coefficient which varies between $\pm 1$ as $N$ changes.

For charged systems, in addition to this number-dependent effect on the kinetic energy, there is also an effect on the potential energy, since the potential is long ranged. To the $1/r$ interaction between two electrons is added the interaction between an electron and all of the images of the other electron. To maintain charge neutrality, an electron must also interact with all of its own images which form a square lattice. Thus, in calculating the potential energy, one term out of $N$ is appropriate to a perfect lattice, not to a Fermi liquid, as it should be. This intuitive result is supported by both Hartree-Fock calculations, valid at small $r_s$, and harmonic lattice calculations, valid at large $r_s$, which shows that the size dependence of the potential energy of the electron gas is proportional to $1/N$.

Taking these contributions into account, the energy per particle for a finite system is assumed to be related to the bulk energy by

$$E_N = E_\infty + b_1(r_s,\xi)\Delta T_N + \frac{b_2(r_s,\xi)}{N} \ . \tag{10}$$

Here, $\Delta T_N$ is the difference between the kinetic energies of $N$ noninteracting electrons and the infinite system at $r_s=1$. The density-dependent parameters $E_\infty$, $b_1$, and $b_2$ were determined by a least-squares fit to VMC calculations at different values of $N$. Specifically, we took $N=26,42,58,72,114$ for the normal fluid and $N=21,37,57,69,113$ for the fully polarized fluid. The

TABLE II. Size dependence in the VMC method of fully-spin-polarized electron fluid at $5 \le r_s \le 75$ and $\chi^2$-fit parameters. Also shown are the GFMC energy and the correlation energy $E_c(r_s,1)$.

| | $r_s=5.0$ | $r_s=10.0$ | $r_s=20.0$ | $r_s=30.0$ | $r_s=40.0$ | $r_s=75.0$ |
|---|---|---|---|---|---|---|
| $N=21$ | −0.2901(2) | −0.169 84(9) | −0.092 67(3) | −0.063 93(1) | −0.048 867(9) | −0.026 914(2) |
| $N=37$ | −0.2863(1) | −0.168 81(8) | −0.092 29(2) | −0.063 774(1) | −0.048 757(8) | −0.026 876(1) |
| $N=57$ | −0.2845(1) | −0.1678(1) | −0.092 14(5) | −0.063 65(1) | −0.048 72(1) | −0.026 855(1) |
| $N=69$ | −0.2862(1) | −0.168 24(6) | −0.092 17(1) | −0.063 705(8) | −0.048 751(4) | −0.026 861(1) |
| $N=113$ | −0.2843(1) | −0.167 93(4) | −0.092 06(1) | −0.063 643(6) | −0.048 711(4) | −0.026 849(1) |
| $E_\infty^{\mathrm{VMC}}$ | −0.2845(1) | −0.1676(1) | −0.091 97(2) | −0.063 62(1) | −0.048 711(7) | −0.026 841(2) |
| $b_1(r_s,1)$ | 0.066(5) | 0.010(4) | 0.0026(7) | 0.0024(3) | 0.0018(3) | 0.000 35(7) |
| $b_2(r_s,1)$ | −0.03(1) | −0.032(6) | −0.011(1) | −0.0032(6) | −0.0008(5) | −0.001 08(1) |
| $\chi^2$ | 11.5 | 5.4 | 0.5 | 1.2 | 2.0 | 0.3 |
| $E_{57}^{\mathrm{GFMC}}$ | −0.285 81(9) | −0.168 53(5) | −0.092 37(2) | −0.063 826(8) | −0.048 841(2) | −0.026 947(3) |
| $E_\infty^{\mathrm{GFMC}}$ | −0.2858(2) | −0.168 07(9) | −0.092 23(2) | −0.063 79(1) | −0.048 844(7) | −0.026 932(3) |
| $10^4\Delta_{\mathrm{MC}}$ | 14.0 | 5.0 | 2.6 | 1.8 | 1.34 | 0.91 |
| $E_c(r_s,1)$ | −0.0263(2) | −0.0183(1) | −0.0123(2) | −0.009 42(1) | −0.007 653(7) | −0.004 652(3) |

TABLE III. Size dependence in the VMC method of the electron crystal at $30 \le r_s \le 100$, and the $\chi^2$-fit parameters. Also shown are the GFMC energies.

| | $r_s=30.0$ | $r_s=40.0$ | $r_s=50.0$ | $r_s=75.0$ | $r_s=100.0$ |
|---|---|---|---|---|---|
| $N=16$ | −0.063 76(3) | −0.048 82(1) | −0.039 622(9) | −0.026 985(4) | −0.020 496(4) |
| $N=30$ | −0.063 65(2) | −0.048 767(9) | −0.039 558(7) | −0.026 960(2) | −0.020 474(3) |
| $N=56$ | −0.063 64(1) | −0.048 749(8) | −0.039 578(8) | −0.026 951(1) | −0.020 477(1) |
| $N=80$ | −0.063 63(1) | −0.048 752(6) | −0.039 566(5) | −0.026 946(2) | −0.020 476(1) |
| $N=120$ | −0.063 64(1) | −0.048 756(6) | −0.039 567(7) | −0.026 941(1) | −0.020 472(1) |
| $E_\infty^{\mathrm{VMC}}$ | −0.063 614(8) | −0.048 745(4) | −0.039 560(4) | −0.026 942(1) | −0.020 473(1) |
| $c(r_s)$ | −0.007(2) | −0.0047(7) | −0.0033(7) | −0.0030(2) | −0.0014(3) |
| $\chi^2$ | 2.0 | 2.5 | 10.8 | 4.2 | 7.6 |
| $E_{56}^{\mathrm{GFMC}}$ | −0.063 778(5) | −0.048 863(5) | −0.039 621(3) | −0.026 988(1) | −0.020 489(1) |
| $E_\infty^{\mathrm{GFMC}}$ | −0.063 760(9) | −0.048 852(6) | −0.039 613(5) | −0.026 981(2) | −0.020 486(2) |
| $10^5\Delta_{\mathrm{MC}}$ | 14.6 | 10.7 | 5.3 | 4.6 | 1.6 |

VMC energies and the $\chi^2$ of the fit as a function of $r_s$ are shown in Table I and Table II for normal and polarized fluids, respectively. The $\chi^2$ of the fit is reasonable, indicating that size dependence is well described by Eq. (10). In some cases the corrections are 60 times larger than the statistical errors, so the $\chi^2$ test is quite severe.

To extract the infinite system GFMC energies, we assume that the size dependence for the variational and the diffusion MC runs are the same. We did GFMC runs only at $N=58$ in the case of normal fluid and $N=57$ in the case of polarized fluid. We then use the previously determined parameters $b_1$ and $b_2$ to determine $E_\infty^{\mathrm{GFMC}}$. In order to check our assumption that the VMC and GFMC runs obey the same finite-size scaling, we have carried out similar calculations with the GFMC method at selective density points, and, indeed, within the statistical errors, found agreement.

To obtain the size dependence of the MC energies in the crystal phase, we use the formula

$$E_N = E_\infty^{\mathrm{VMC}} + \frac{c(r_s)}{N^{3/2}} , \tag{11}$$

which becomes valid in the strong-coupling limit (viz., $r_s \gg 1$). We have performed VMC runs at $N=16,30,56,80,120$ to determine the parameter $c(r_s)$ and used the aforementioned procedure to extract the infinite system energies in the GFMC method. The results are shown in Table III.

## IV. GROUND-STATE ENERGY

Having determined the finite-size corrections to the MC energies, we now turn to the problem of obtaining the equation of state of the electron gas. The ground-state energy of the interacting-electron system in the liquid phase as a function of the density parameter $r_s$, and the degree of polarization $\xi$, can be written as

$$E(r_s,\xi) = E_{\mathrm{HF}}(r_s,\xi) + E_c(r_s,\xi) , \tag{12}$$

where the Hartree-Fock energy consists of the kinetic-energy term and the exchange energy,

$$E_{\mathrm{HF}}(r_s,\xi) = \frac{1+\xi^2}{r_s^2} + \frac{4\sqrt{2}}{3\pi r_s}[(1+\xi)^{3/2}+(1-\xi)^{3/2}] . \tag{13}$$

In order to fit the energy to a functional form, we assume the correlation energy, $E_c$, can be approximated by

$$E_c(r_s,\xi) = a_0 \frac{1+a_1 x}{1+a_1 x + a_2 x^2 + a_3 x^3} , \tag{14}$$

where $x=(r_s)^{1/2}$ and the parameters $a_i(\xi)$ in this Padé approximant are determined by a nonlinear least-squares fit to the MC data at the density values $r_s=1,5,10,15,20,30,50$ for the normal fluid phase and $r_s=1,5,10,15,20,30,40,50,75$ for the spin-polarized fluid. This Padé form behaves like $\sim a+br_s$ as $r_s \to 0$, which has the correct high-density expansion short of the $r_s \ln r_s$ term, and admits the asymptotic form

$$E \sim \frac{a}{r_s} + \frac{b}{r_s^{3/2}} + \frac{c}{r_s^2} + \cdots \tag{15}$$

as $r_s \to \infty$. The parameters giving the best fit for the normal and fully polarized liquids are given in Table IV.

There is a discrepancy in the earlier calculations[4,5] of the correlation energy at $r_s=0$, $E_c(0,0)$, and a prediction for this quantity is provided by means of our fitting pa-

TABLE IV. Parameters of the Padé approximants [Eq. (14)] to the correlation energy determined by least-squares fitting for normal and polarized fluids (Tables I and II) and parameters of the fit [Eq. (15)] to the energy of the crystal phase.

| | Fluid | |
|---|---|---|
| | Normal | Polarized |
| $a_0$ | −0.3568 | −0.0515 |
| $a_1$ | 1.1300 | 340.5813 |
| $a_2$ | 0.9052 | 75.2293 |
| $a_3$ | 0.4165 | 37.0170 |
| | Crystal | |
| $c_1$ | $c_{3/2}$ | $c_2$ |
| −2.2122 | 1.6284 | 0.0508 |

rameter $a_0$ in Eq. (14). We calculate $a_0=-0.357$ (see Table IV), which is in agreement with the Rajagopal-Kimball[4] result of $-0.38\pm0.04$ and close to the coupled-cluster ladder-approximation value of Freeman[10] of $-0.39$. On the other hand, Isihara and Toyoda[5] find the correlation energy at infinite density to be $-0.6258\pm0.002$. If in the Padé approximant [Eq. (14)] we fix the value of $a_0$ to be $-0.39$, the resulting $\chi^2$ increases from 6.6 to 9.0 with very little change in the remaining parameters $a_i$. Thus our results are well fitted by the assumed functional form even when the Freeman value at high density is used as a constraint.

The calculated MC energies at several densities are compared with other theoretical calculations in Fig. 1. Our calculated ground-state energy is consistently lower than the cluster-expansion calculation of Sim *et al.*[12] (indicated with the dotted line). They use a parametrized $g(r)$ in the hypernetted-chain approximation, along with the Wu-Feenberg expansion for the trial wave function. We also display two calculations by Freeman[7,10]—one based on the ring approximation (which is rather poor), the other on the coupled-cluster and ladder approximations. The calculation of Jonson[3] is an application of the Singwi-Tosi-Land-Sjölander (STLS) scheme to the two-dimensional case. The Ioriatti-Isihara[9] calculation (dashed curve), where they use analytical continuation to obtain the intermediate- to low-density expansion gives a much higher energy than any other calculation. The fixed-node approximation made here gives an upper bound to the ground-state energy. Thus any result with an even higher energy can be ruled out. None of the other theoretical calculations are very accurate for $r_s>2$, where the potential energy dominates. Note that, at low density, calculations can give rather similar correlation energies and still be inaccurate since the largest part of the correlation energy will be a static Madelung term. Instead, energy differences at low densities should be compared to relative to a typical kinetic energy in the problem; we prefer the zero-point energy of a harmonic lattice, which is $1.63r_s^{-3/2}$.

The energy in the crystal phase is expected[6] to have the form

$$E(r_s)=\frac{c_1}{r_s}+\frac{c_{3/2}}{r_s^{3/2}}+\frac{c_2}{r_s^2}+\cdots\ , \tag{16}$$

where the harmonic coefficient is known to be[21] $c_1=-2.2122$ and the second coefficient is approximately $c_{3/2}=1.63$. Using a constrained least-squares fit to the MC energies in the crystal phase, we determine the coefficients of the higher-order anharmonic terms. The MC points used to extract $c_{3/2}$ and $c_2$ in Eq. (16) are at $r_s=30,40,50,75,100$. Our value for $c_{3/2}$ is 1.628.

Our calculations were done with like spins in alternating lines. Since the triangular lattice is not bipartite, such an arrangement is not antiferromagnetic. We tried some other arrangements of spins such as bosons (no antisymmetry) and a ferromagnetic arrangement. All arrangements of spins had the same energy at $r_s=40$ within the statistical errors. Path-integral calculations of the tunneling frequencies of electrons in a 2D Wigner crystal similar to those recently done with solid $^3$He are in pro-

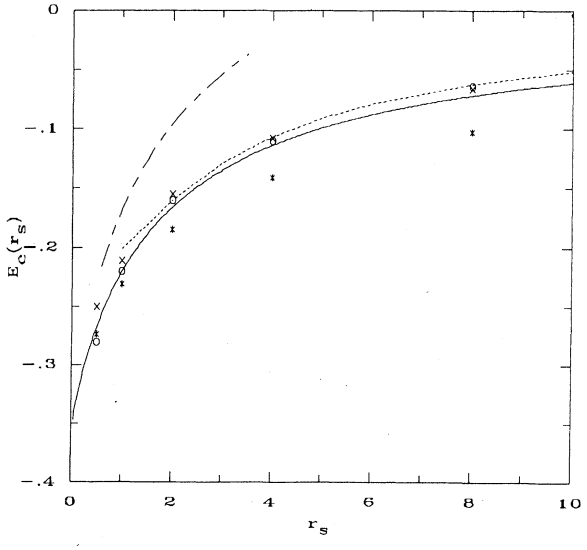


FIG. 1. The correlation energy, $E_c(r_s,0)$ (in units of Rydbergs/per electron) of the 2D electron gas in the normal fluid phase (solid curve) compared with other theoretical calculations. The dashed (-----) curve is from Ioriatti and Isihara (Ref. 9). The short-dashed curve is that of Sim *et al.* (Ref. 12). Also shown are the results of Freeman in the ring approximation (*, Ref. 7) and coupled-cluster ladder approximation (○, Ref. 10). × indicates the STLS calculation of Jonson (Ref. 3).

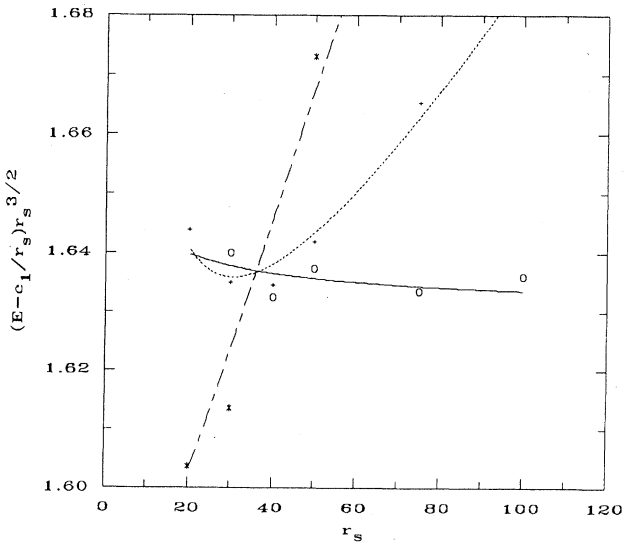


FIG. 2. The ground-state energy, $E(r_s,\xi)$ of the electron gas in the normal (dashed) and the fully-spin-polarized fluids (dotted), and in the crystal phase (solid) as a function of the density parameter $r_s$. $c_1$ is the Madelung constant. We have subtracted out the Madelung energy and multiplied by $r_s^{3/2}$. The MC points with associated error bars are indicated as follows: ○, crystal; *, normal fluid; +, polarized fluid. The curves are fitted to the points with Eqs. (14) and (16).

gress.[22] Roger has predicted that the lowest-energy arrangement of spins is ferromagnetic since he expects that three-electron exchange will dominate.[23]

In Fig. 2, $T=(E-c_1/r_s)r_s^{3/2}$ is plotted for all three phases at low density. Here, $c_1=-2.2122$ is the coefficient of the static energy term in Eq. (16); thus, $T$ is proportional to the difference in energy from the static Madelung energy divided by the typical kinetic energy. We observe from the graph that the electron system crystallizes at the density $r_s \simeq 37 \pm 5$, and this transition occurs between the normal fluid phase and the crystal phase. This is an electron density of $8.3\times10^{12}/\text{cm}^2$. From Tables I and II we notice that $E^{\text{VMC}}(r_s,0)$ and $E^{\text{VMC}}(r_s,1)$ intersect in the region $10 \le r_s \le 20$, which is consistent with earlier VMC results.[6] The more accurate GFMC calculation does not predict a transition to the ferromagnetic state. There is no transition from the normal fluid (paramagnetic) phase to the polarized fluid (ferromagnetic) phase since Wigner crystallization occurs at roughly the same density. Note, however, that all phases have approximately equal energies at $r_s=40$. Very interesting behavior of the 2D electron gas may occur near this density as a function of temperature and magnetic field. Of course, the present calculations cannot resolve the nature of the phase transitions or predict exactly which phase will be stable at $r_s \approx 37$, since, first of all, finite system effects are important, and secondly, the fixed-node approximation has been used.

Our crystallization density is consistent with that found at finite temperatures by Imada and Takahashi.[13] They did path-integral simulations of spinless fermions at temperatures down to 20 K, which corresponds to an energy in our units of $2\times10^{-4}$ Ry. Their method of treating fermions did not allow them to examine the fermion liquids at lower temperatures.

Tables I–III gives the difference between the variational energy and the fixed-node energy in the three phases we have examined. In the high-density liquid the Jastrow wave function picks up 90% of the correlation energy in the unpolarized liquid and 95% in the polarized liquid, while the crystal trial function picks up 98% of the zero-

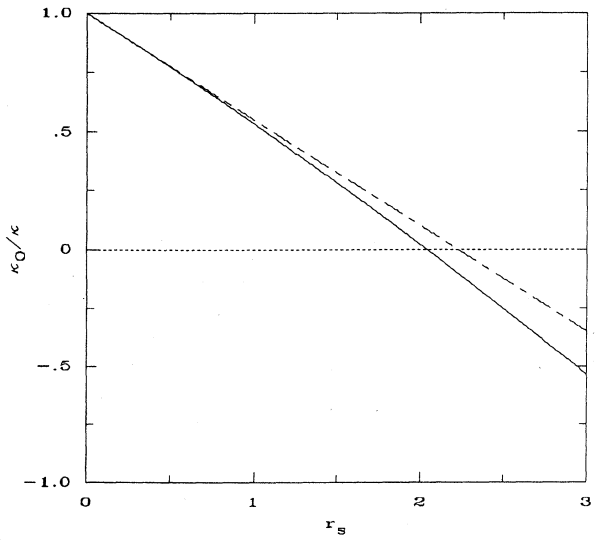


FIG. 3. The compressibility $\kappa_0/\kappa$ of the electron gas as function of density parameter $r_s$, calculated using Eq. (17). Dashed line is the compressibility in the Hartree-Fock approximation.

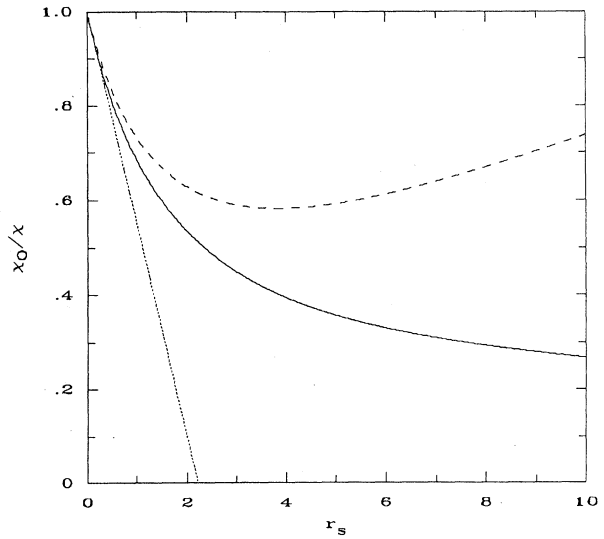


FIG. 4. The spin susceptibility $\chi_0/\chi$ of the electron gas as a function of the density parameter $r_s$, calculated using interpolation based on the correlation energy, Eq. (18) (dashed line), and using interpolation based on the total energy, Eq. (20) (solid line). Dotted line is the Hartree-Fock result.

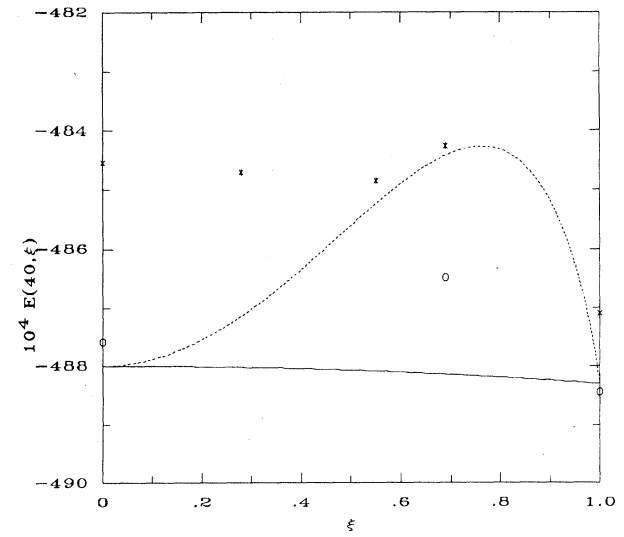


FIG. 5. The ground-state energy as a function of polarization $\xi$ at $r_s=40$. Shown are the GFMC points (○) at polarizations of 0%, 69%, and 100%, and VMC points (*) at polarizations of 0%, 28%, 55%, and 69%. The dotted curve is obtained by interpolating the correlation energy of the two end points and the solid line is obtained by interpolating on the total energy. The curves do not go through the circles at $\xi=0$ and 1 because they are computed using Eq. (14), which is fitted to the energies at other densities as well.

point motion. Roughly speaking, the polarized trial function is twice as good as the unpolarized trial function, while the crystal trial function is best of all; it is twice as good as the polarized-liquid function. In general, it is easier to write down a good trial function for an ordered phase than for a disordered one. Because of this, phase-transition densities computed with variational methods can be quite different from the exact values.

Having obtained the equation of state [i.e., $E(r_s)$] of the normal liquid, we calculate the compressibility using

$$\frac{\kappa_0}{\kappa}=1-\frac{\sqrt{2}r_s}{\pi}+\frac{r_s^4}{8}\left[\frac{d^2}{dr_s^2}-\frac{1}{r_s}\frac{d}{dr_s}\right]E_c \ . \tag{17}$$

Here, $\kappa_0=\pi r_s^4/2$ is the compressibility of a noninteracting system (see Fig. 3). In the above formula, the compressibility becomes negative around $r_s\sim 2.03$, in contrast with the Hartree-Fock result of 2.22. Stability at low density is achieved in physical systems by the background.

The total spin susceptibility may be expressed as

$$\frac{\chi_0}{\chi}=1-\frac{\sqrt{2}}{\pi}r_s+\frac{r_s^2}{2}\frac{\partial^2 E_c}{\partial\xi^2}\bigg|_{\xi=0} , \tag{18}$$

where $\chi_0$ is the noninteracting susceptibility. The last term also defines the spin-stiffness coefficient,

$$\alpha_c(r_s)=\frac{\partial^2 E_c(r_s,\xi)}{\partial\xi^2}\bigg|_{\xi=0} . \tag{19}$$

It is difficult in the Monte Carlo method to directly calculate the spin susceptibility, since for a simple calculation of the finite-size effects one must flip an entire *shell* of spins and the polarization will change by a large amount (say 25%). At high density one expects that the correlation energy should interpolate smoothly between zero polarization and full polarization. Then one can obtain an estimate of the susceptibility from the MC-determined energies by assuming that the correlation energy is a quadratic function of the polarization and applying Eq. (19). That is shown as the dashed line in Fig. 4. It shows a minimum around $r_s\approx 3.5$ and then grows at large $r_s$. Also shown in the same figure is the Hartree-Fock approximation to $\chi_0/\chi$.

On the other hand, at large $r_s$ the Hartree-Fock reference state is very different from the true ground state, so one does not expect the correlation energy to have much relevance. So another estimate of the susceptibility comes from assuming that the total energy is a quadratic function of the polarization,

$$\frac{\chi_0}{\chi}\approx r_s^2[E(r_s,1)-E(r_s,0)] . \tag{20}$$

This is shown as the solid curve and will vanish at $r_s=37$ since the polarized and unpolarized liquids have the same energy (see Fig. 2).

At the freezing density we have performed some calculations at intermediate polarizations to determine which method of interpolation is more accurate at low density, and to examine the possibility that intermediate polarization could have lower energies than either fully polarized or unpolarized systems. The result is shown in Fig. 5. Shown in the same graph are the results of VMC calculations for partial polarizations $\xi=0.28,0.55,0.69$, and a GFMC calculation at $\xi=0.69$ (i.e., $N_\uparrow=49$, $N_\downarrow=9$ in a 58-particle system). The MC energies are corrected for the finite-size effects by interpolating between the values at zero and full polarizations:

$$b_i(r_s,\xi)=b_i(r_s,0)+\xi^2[b_i(r_s,1)-b_i(r_s,0)] . \tag{21}$$

It is seen that the partially polarized energy lies between the result obtained by interpolating on the correlation energy or on the total energy. However, the energy of in-

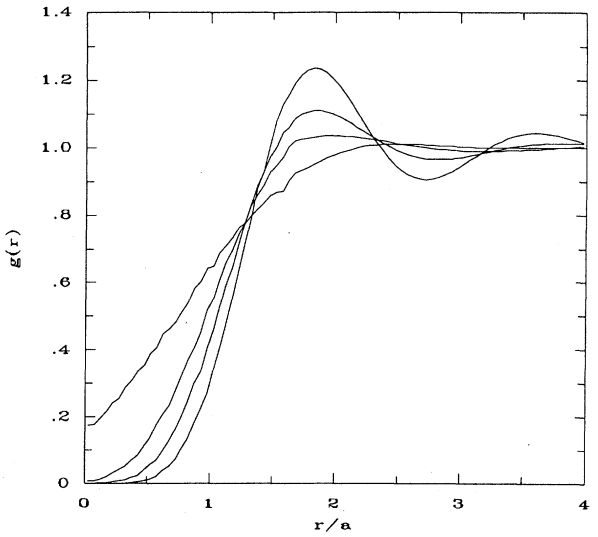


FIG. 6. The extrapolated pair distribution function $g(r)$ of the electron gas in the unpolarized fluid phase, at densities $r_s=1,5,10,20$. The larger $r_s$ values have larger oscillations.

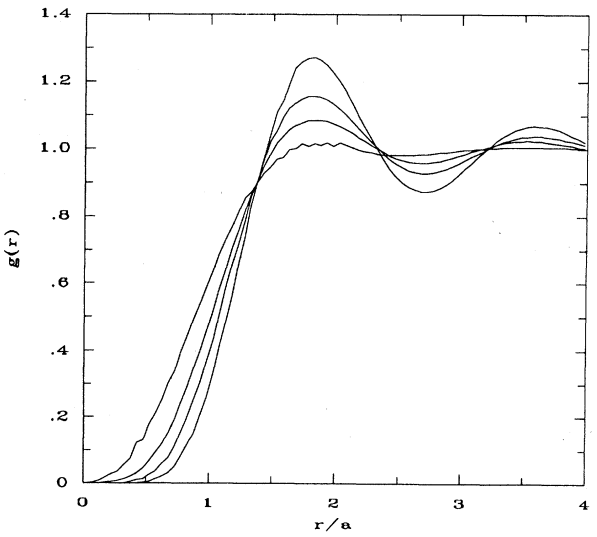


FIG. 7. The extrapolated pair distribution function $g(r)$ of the electron gas in the fully-spin-polarized fluid phase, at densities $r_s=1,5,10,20$.

termediate polarization is higher than the other two (interpolation on correlation energy and total energy), indicating that the electron gas in two dimensions does not pass through a phase of partial polarization. We suspect that this ordering holds at all densities, so the two methods of determining the spin susceptibility will give upper and lower bounds, and that the true result is roughly halfway in between. Figure 5 also shows that variational Jastrow calculations will predict that the electron gas would be ferromagnetic at $r_s=40$. This is analogous to the situation in liquid $^3$He.

## V. STATIC PROPERTIES

The variational and Green's-function Monte Carlo methods yield information about other microscopic properties of the system as well, most notably, the radial pair distribution function,

$$g(\mathbf{r})=\frac{1}{N}\sum_{\substack{i,j=1\\(i\neq j)}}\langle\delta^2(\mathbf{r}_i-\mathbf{r}_j-\mathbf{r})\rangle\ , \tag{22}$$

and its Fourier transform, the static structure factor

$$S(\mathbf{k})=1+\frac{\rho}{2}\int d\mathbf{r}\, e^{i\mathbf{k}\cdot\mathbf{r}}[g(\mathbf{r})-1]\ . \tag{23}$$

Strictly speaking, the radial pair distribution function, $g_M(r)$, calculated with the converged (mixed) distribution

TABLE V. The extrapolated radial pair distribution function $g(r)$ for the densities $r_s=1,5,10,20$ in the normal fluid phase. The errors are between 0.01 and 0.005.

| | $g(r)$ | | | |
|---|---|---|---|---|
| $\frac{r}{a}$ | $r_s=1.0$ | $r_s=5.0$ | $r_s=10.0$ | $r_s=20.0$ |
| 0.025 | 0.176 | 0.009 | 0.000 | 0.000 |
| 0.125 | 0.197 | 0.014 | 0.003 | 0.000 |
| 0.225 | 0.243 | 0.030 | 0.006 | 0.000 |
| 0.325 | 0.289 | 0.051 | 0.011 | 0.001 |
| 0.425 | 0.338 | 0.085 | 0.023 | 0.005 |
| 0.525 | 0.387 | 0.137 | 0.058 | 0.014 |
| 0.625 | 0.447 | 0.208 | 0.097 | 0.039 |
| 0.725 | 0.484 | 0.279 | 0.166 | 0.073 |
| 0.825 | 0.540 | 0.369 | 0.249 | 0.133 |
| 0.925 | 0.605 | 0.452 | 0.334 | 0.225 |
| 1.025 | 0.649 | 0.554 | 0.462 | 0.344 |
| 1.125 | 0.710 | 0.659 | 0.593 | 0.476 |
| 1.225 | 0.763 | 0.743 | 0.715 | 0.636 |
| 1.325 | 0.796 | 0.828 | 0.829 | 0.786 |
| 1.425 | 0.834 | 0.888 | 0.926 | 0.929 |
| 1.525 | 0.867 | 0.947 | 1.002 | 1.082 |
| 1.625 | 0.902 | 1.002 | 1.057 | 1.157 |
| 1.725 | 0.938 | 1.017 | 1.091 | 1.217 |
| 1.825 | 0.950 | 1.035 | 1.101 | 1.226 |
| 1.925 | 0.972 | 1.034 | 1.114 | 1.196 |
| 2.025 | 0.979 | 1.045 | 1.089 | 1.187 |
| 2.125 | 0.987 | 1.028 | 1.071 | 1.130 |
| 2.225 | 1.013 | 1.031 | 1.059 | 1.069 |
| 2.325 | 1.001 | 1.025 | 1.018 | 1.014 |
| 2.425 | 1.007 | 1.012 | 1.000 | 0.967 |
| 2.525 | 1.002 | 1.008 | 0.990 | 0.924 |
| 2.625 | 1.010 | 0.996 | 0.962 | 0.905 |
| 2.725 | 1.010 | 0.998 | 0.974 | 0.900 |
| 2.825 | 1.007 | 0.988 | 0.971 | 0.912 |
| 2.925 | 1.001 | 0.997 | 0.963 | 0.920 |
| 3.025 | 1.003 | 0.992 | 0.982 | 0.941 |
| 3.125 | 1.000 | 0.982 | 0.966 | 0.976 |
| 3.225 | 0.933 | 0.994 | 0.993 | 0.989 |
| 3.325 | 0.990 | 0.993 | 0.993 | 1.025 |
| 3.425 | 0.996 | 0.999 | 1.009 | 1.035 |
| 3.525 | 0.993 | 0.988 | 1.007 | 1.038 |
| 3.625 | 0.995 | 0.991 | 1.017 | 1.043 |
| 3.725 | 0.995 | 0.996 | 1.016 | 1.093 |
| 3.825 | 0.998 | 0.996 | 1.018 | 1.027 |
| 3.925 | 0.992 | 1.002 | 1.008 | 1.016 |

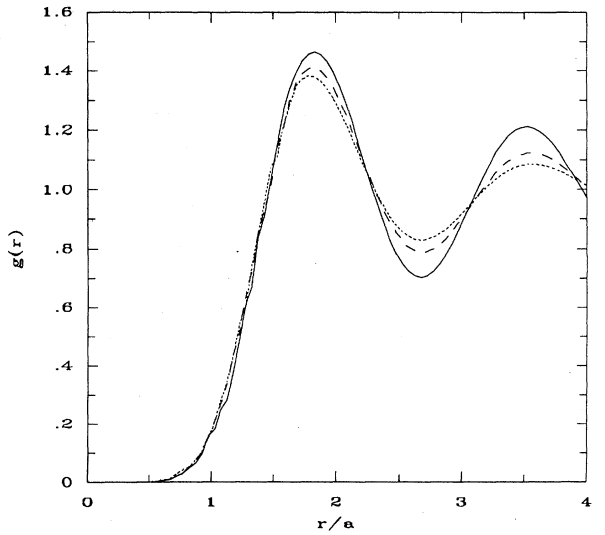


FIG. 8. The extrapolated pair distribution function $g(r)$ of the electron gas in the crystal phase (solid), fully polarized fluid phase (dashed), and normal fluid phase (dotted) at $r_s=40$.

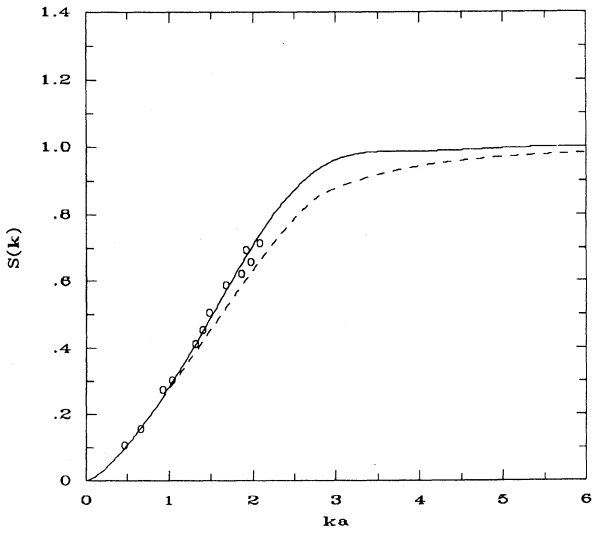


FIG. 9. The static structure factor $S(k)$ of the electron gas in the normal fluid phase at $r_s=1$. The circles are the direct MC evaluation of the structure factor [Eq. (27)], the solid curve is the Fourier transform of the pair correlation function [Eq. (26)], and the dashed curve is the MSA $S(k)$ [Eq. (29)].

$\phi(R)\psi(R)$ in the GFMC method, lies somewhere between the variational distribution function $g_V(r)$ and the exact (fixed-node) one. Assuming that the trial wave function is sufficiently accurate, $g_M(r)$ should be halfway[24] between $g_V(r)$ and exact $g(r)$:

$$g(r)\approx 2g_M(r)-g_V(r) \ . \tag{24}$$

This expression is correct to first order in $\phi(R)-\psi(R)$.

The pair correlation function $g(r)$ as calculated in the MC simulations is fitted to an assumed functional form,

$$g_A(r)=1+m_1\frac{e^{-m_2 r}}{r}\cos(m_3 r+m_4) \ , \tag{25}$$

TABLE VI. The extrapolated radial pair distribution function $g(r)$ for the densities $r_s=1,5,10,20$ in the spin-polarized fluid phase. The errors are between 0.01 and 0.005.

| | $g(r)$ | | | |
|---|---|---|---|---|
| $\frac{r}{a}$ | $r_s=1.0$ | $r_s=5.0$ | $r_s=10.0$ | $r_s=20.0$ |
| 0.025 | 0.000 | 0.000 | 0.000 | 0.000 |
| 0.125 | 0.007 | 0.003 | 0.000 | 0.000 |
| 0.225 | 0.030 | 0.007 | 0.001 | 0.000 |
| 0.325 | 0.057 | 0.020 | 0.002 | 0.001 |
| 0.425 | 0.124 | 0.040 | 0.014 | 0.001 |
| 0.525 | 0.177 | 0.084 | 0.036 | 0.007 |
| 0.625 | 0.252 | 0.135 | 0.074 | 0.025 |
| 0.725 | 0.342 | 0.224 | 0.127 | 0.062 |
| 0.825 | 0.445 | 0.312 | 0.212 | 0.126 |
| 0.925 | 0.541 | 0.411 | 0.314 | 0.208 |
| 1.025 | 0.639 | 0.527 | 0.429 | 0.321 |
| 1.125 | 0.729 | 0.629 | 0.587 | 0.463 |
| 1.225 | 0.813 | 0.752 | 0.697 | 0.629 |
| 1.325 | 0.870 | 0.851 | 0.845 | 0.807 |
| 1.425 | 0.927 | 0.935 | 0.945 | 0.952 |
| 1.525 | 0.968 | 1.003 | 1.038 | 1.102 |
| 1.625 | 0.996 | 1.036 | 1.137 | 1.195 |
| 1.725 | 1.015 | 1.086 | 1.174 | 1.263 |
| 1.825 | 1.014 | 1.071 | 1.149 | 1.275 |
| 1.925 | 1.016 | 1.068 | 1.148 | 1.259 |
| 2.025 | 1.004 | 1.060 | 1.126 | 1.194 |
| 2.125 | 1.001 | 1.049 | 1.058 | 1.113 |
| 2.225 | 0.994 | 1.028 | 1.051 | 1.071 |
| 2.325 | 0.989 | 1.004 | 0.992 | 1.001 |
| 2.425 | 0.981 | 0.977 | 0.981 | 0.929 |
| 2.525 | 0.979 | 0.960 | 0.940 | 0.908 |
| 2.625 | 0.973 | 0.957 | 0.924 | 0.892 |
| 2.725 | 0.982 | 0.959 | 0.912 | 0.877 |
| 2.825 | 0.982 | 0.962 | 0.935 | 0.888 |
| 2.925 | 0.984 | 0.967 | 0.960 | 0.895 |
| 3.025 | 0.993 | 0.985 | 0.964 | 0.938 |
| 3.125 | 0.991 | 0.993 | 0.992 | 0.967 |
| 3.225 | 1.005 | 1.004 | 1.003 | 1.011 |
| 3.325 | 1.010 | 1.009 | 1.014 | 1.033 |
| 3.425 | 1.002 | 1.007 | 1.026 | 1.053 |
| 3.525 | 1.006 | 1.024 | 1.048 | 1.070 |
| 3.625 | 1.001 | 1.023 | 1.034 | 1.069 |
| 3.725 | 0.998 | 1.019 | 1.032 | 1.059 |
| 3.825 | 0.999 | 1.014 | 1.029 | 1.034 |
| 3.925 | 0.996 | 0.999 | 1.016 | 1.024 |

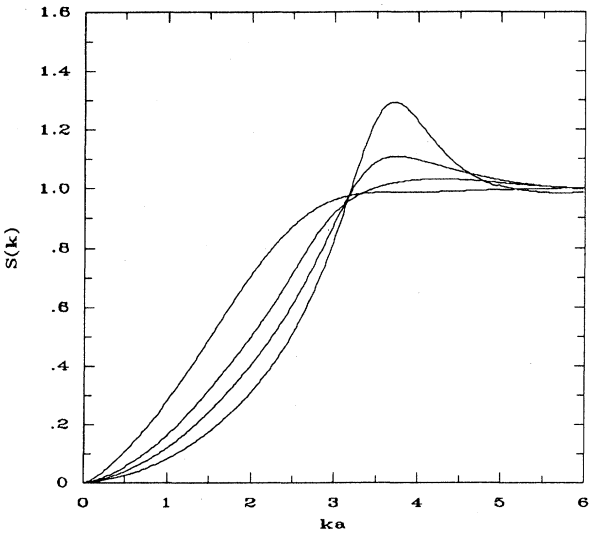


FIG. 10. The static structure factor $S(k)$ of the electron gas in the normal fluid phase at densities $r_s=1,5,10,20$.

to determine the large-$r$ behavior and to Fourier transform it.

We show the pair distribution function $g(r)$ for the electron gas in the normal fluid phase in Fig. 6, and in the fully polarized phase in Fig. 7, at densities $r_s=1,5,10,20$. We have also tabulated the numerical values of $g(r)$ at these densities in Tables V and VI. Also shown, in Fig. 8, is the $g(r)$ of all three phases, at $r_s=40$ near the Wigner melting. Although the energies of the three phases are virtually the same, the pair correlations differ by about 5%.

The static structure factor is then calculated by Fourier transformation,

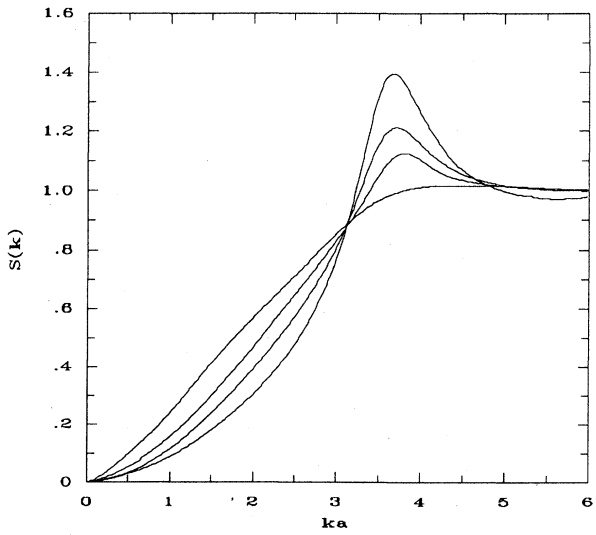


FIG. 11. The static structure factor $S(k)$ of the electron gas in the fully-spin-polarized fluid phase at densities $r_s=1,5,10,20$.

$$S(k)=1+2\pi\rho\int_0^\infty dr\, rJ_0(kr)[g(r)-1]\ , \tag{26}$$

where $J_0(kr)$ is the zeroth-order Bessel function of the first kind. $S(k)$ is also calculated directly by

$$S(k)=\frac{1}{N}\sum_{\sigma_1,\sigma_2}\langle\rho^\dagger_{\mathbf{k}\sigma_1}\rho_{\mathbf{k}\sigma_2}\rangle \tag{27}$$

using the configurations generated by the MC runs where the density operator is

$$\rho_{\mathbf{k}\sigma_1}=\sum_{i=1}^{N}\delta_{\sigma_1\sigma_i}e^{i\mathbf{k}\cdot\mathbf{r}_i}\ , \tag{28}$$

and the agreement between this direct $S(k)$ and the one constructed by the Fourier transform is good, as can be seen in Fig. 9. On the same figure we also show the structure factor proposed in the mean spherical approximation (MSA),

$$S(k)=\left[\frac{1}{S_0(k)^2}+\frac{4v(k)m}{\hbar^2k^2}\right]^{-1/2}\ , \tag{29}$$

which gives the correct behavior for small $k$ [i.e., in the RPA limit $S(k)\sim k^{3/2}$]. The MSA structure factor and the MC structure factor agree up to the Fermi wave vector ($k_F=\sqrt{2}$) at this value of $r_s$. At low densities (i.e., $r_s\gg1$) the MSA structure factor is adequate only for smaller values of $k$.

The computed structure factors are displayed in Figs. 10 and 11 for the normal and spin-polarized electron gases at densities $r_s=1,5,10,20$. The numerical values of $S(k)$ at these densities are shown in Tables VII and VIII.

Another quantity of interest is the one-body density matrix,

$$\rho_1(\mathbf{r})=\langle\psi(\mathbf{r}_1+\mathbf{r})/\psi(\mathbf{r}_1)\rangle$$
$$=\int\psi^*(\mathbf{r}_1+\mathbf{r},\mathbf{r}_2,\ldots)\psi(\mathbf{r}_1,\mathbf{r}_2,\ldots)d\mathbf{r}_1\cdots d\mathbf{r}_N\ , \tag{30}$$

where the average is taken over the configurations $R$ and over the electron to displace the diagonal. The momentum distribution $n(k)$ is then the Fourier transform of the one-body density matrix:

$$n(k)=\rho\int d\mathbf{r}\,\rho_1(\mathbf{r})e^{i\mathbf{k}\cdot\mathbf{r}}\ . \tag{31}$$

This is calculated by inserting a *ghost* electron at random, uniformly in the box, and determining how the wave function changes.[16] However, $n(k)$ may also be evaluated directly according to the formula

$$n(k)=\left\langle e^{i\mathbf{k}\cdot(\mathbf{r}'-\mathbf{r}_i)}\frac{\psi(\mathbf{r}')}{\psi(\mathbf{r}_i)}\right\rangle\ . \tag{32}$$

TABLE VII. The extrapolated static structure factor $S(k)$ of the normal fluid phase for four densities. These were determined by extending the radial distribution functions according to Eq. (25) and Fourier transforming.

| | $S(k)$ | | | |
|---|---|---|---|---|
| $ka$ | $r_s=1.0$ | $r_s=5.0$ | $r_s=10.0$ | $r_s=20.0$ |
| 0.2 | 0.030 | 0.014 | 0.010 | 0.007 |
| 0.4 | 0.080 | 0.039 | 0.028 | 0.019 |
| 0.6 | 0.140 | 0.074 | 0.053 | 0.034 |
| 0.8 | 0.206 | 0.115 | 0.083 | 0.056 |
| 1.0 | 0.284 | 0.165 | 0.121 | 0.083 |
| 1.2 | 0.364 | 0.222 | 0.165 | 0.116 |
| 1.4 | 0.449 | 0.286 | 0.217 | 0.155 |
| 1.6 | 0.538 | 0.354 | 0.273 | 0.199 |
| 1.8 | 0.625 | 0.425 | 0.336 | 0.251 |
| 2.0 | 0.708 | 0.501 | 0.404 | 0.311 |
| 2.2 | 0.783 | 0.581 | 0.480 | 0.381 |
| 2.4 | 0.847 | 0.668 | 0.564 | 0.464 |
| 2.6 | 0.898 | 0.762 | 0.660 | 0.564 |
| 2.8 | 0.936 | 0.850 | 0.768 | 0.685 |
| 3.0 | 0.962 | 0.918 | 0.884 | 0.832 |
| 3.2 | 0.977 | 0.963 | 0.991 | 1.003 |
| 3.4 | 0.984 | 0.992 | 1.066 | 1.171 |
| 3.6 | 0.986 | 1.011 | 1.102 | 1.277 |
| 3.8 | 0.986 | 1.022 | 1.107 | 1.285 |
| 4.0 | 0.987 | 1.028 | 1.096 | 1.225 |
| 4.2 | 0.988 | 1.031 | 1.081 | 1.154 |
| 4.4 | 0.989 | 1.030 | 1.065 | 1.095 |
| 4.6 | 0.991 | 1.027 | 1.050 | 1.053 |
| 4.8 | 0.993 | 1.023 | 1.038 | 1.022 |
| 5.0 | 0.995 | 1.019 | 1.027 | 1.007 |
| 5.2 | 0.997 | 1.014 | 1.018 | 0.996 |
| 5.4 | 0.998 | 1.009 | 1.011 | 0.989 |
| 5.6 | 0.999 | 1.005 | 1.005 | 0.983 |
| 5.8 | 1.000 | 1.002 | 1.000 | 0.984 |

TABLE VIII. The static structure factor $S(k)$ of the spin-polarized fluid phase for four densities.

| | $S(k)$ | | | |
|---|---|---|---|---|
| $ka$ | $r_s=1.0$ | $r_s=5.0$ | $r_s=10.0$ | $r_s=20.0$ |
| 0.2 | 0.028 | 0.014 | 0.009 | 0.007 |
| 0.4 | 0.073 | 0.038 | 0.023 | 0.020 |
| 0.6 | 0.140 | 0.069 | 0.045 | 0.039 |
| 0.8 | 0.178 | 0.111 | 0.077 | 0.061 |
| 1.0 | 0.240 | 0.158 | 0.115 | 0.089 |
| 1.2 | 0.308 | 0.209 | 0.160 | 0.121 |
| 1.4 | 0.378 | 0.267 | 0.212 | 0.159 |
| 1.6 | 0.445 | 0.332 | 0.267 | 0.202 |
| 1.8 | 0.508 | 0.398 | 0.328 | 0.250 |
| 2.0 | 0.567 | 0.466 | 0.391 | 0.304 |
| 2.2 | 0.624 | 0.538 | 0.459 | 0.365 |
| 2.4 | 0.680 | 0.610 | 0.532 | 0.436 |
| 2.6 | 0.738 | 0.680 | 0.611 | 0.521 |
| 2.8 | 0.797 | 0.755 | 0.701 | 0.627 |
| 3.0 | 0.855 | 0.831 | 0.808 | 0.770 |
| 3.2 | 0.906 | 0.910 | 0.938 | 0.963 |
| 3.4 | 0.949 | 1.002 | 1.089 | 1.208 |
| 3.6 | 0.980 | 1.088 | 1.195 | 1.382 |
| 3.8 | 1.000 | 1.125 | 1.203 | 1.365 |
| 4.0 | 1.011 | 1.103 | 1.153 | 1.260 |
| 4.2 | 1.016 | 1.065 | 1.105 | 1.166 |
| 4.4 | 1.017 | 1.042 | 1.069 | 1.093 |
| 4.6 | 1.016 | 1.029 | 1.044 | 1.048 |
| 4.8 | 1.016 | 1.019 | 1.028 | 1.017 |
| 5.0 | 1.014 | 1.015 | 1.017 | 0.997 |
| 5.2 | 1.012 | 1.012 | 1.010 | 0.985 |
| 5.4 | 1.009 | 1.008 | 1.006 | 0.976 |
| 5.6 | 1.006 | 1.006 | 1.002 | 0.973 |
| 5.8 | 1.003 | 1.005 | 1.000 | 0.974 |

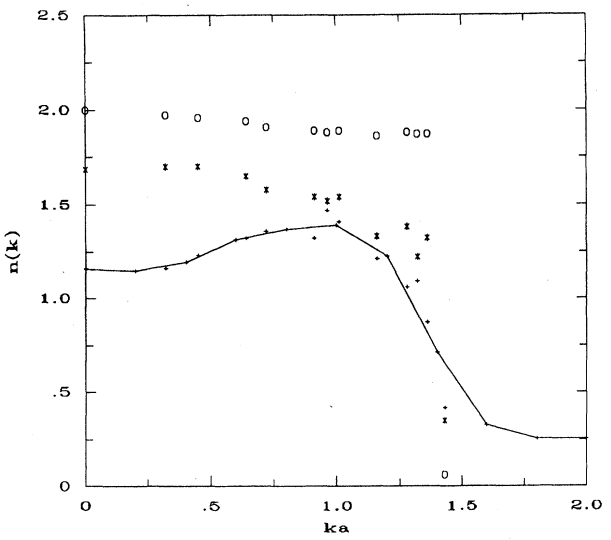


FIG. 12. The momentum distribution $n(k)$ of the electron gas in the normal fluid phase at densities $r_s=1$ (○), 5 (*), and 10 (+). The solid line represents the Fourier transform of the one-body density matrix at $r_s=10$.

where $\mathbf{r}'$ is the position of the *ghost* electron. These two methods do not give identical results in finite systems because Fourier transforming and sphericalizing do not commute. In Fig. 12 and Table IX we display and list the momentum distributions for the unpolarized-electron liquid calculated variationally for an $N=122$ particle system at densities $r_s=1,5,10$. Also shown is the Fourier transform of the one-body density matrix for $r_s=10$, and we observe that the agreement with the direct calculation is good. The normalization is such that for an ideal unpolarized spin $\frac{1}{2}$ liquid the momentum distribution will be 2 for states inside the Fermi wave vector and zero outside. Our computed momentum distribution at $r_s=1$ is close to the ideal distribution. At $r_s=2$ the discontinuity at the Fermi surface has dropped considerably. At

TABLE IX. The variational momentum distribution $n(k)$ of the normal fluid phase for the densities $r_s=1,5,10$ as calculated using Eq. (32).

| | $n(k)$ | | |
|---|---|---|---|
| $ka$ | $r_s=1.0$ | $r_s=5.0$ | $r_s=10.0$ |
| 0.00 | 2.00 | 1.69 | 1.16 |
| 0.32 | 1.97 | 1.70 | 1.16 |
| 0.45 | 1.96 | 1.70 | 1.23 |
| 0.64 | 1.94 | 1.65 | 1.32 |
| 0.72 | 1.91 | 1.58 | 1.36 |
| 0.91 | 1.89 | 1.54 | 1.32 |
| 0.96 | 1.88 | 1.52 | 1.47 |
| 1.01 | 1.89 | 1.54 | 1.41 |
| 1.16 | 1.86 | 1.33 | 1.21 |
| 1.28 | 1.88 | 1.38 | 1.06 |
| 1.32 | 1.87 | 1.22 | 1.09 |
| 1.36 | 1.87 | 1.32 | 0.87 |
| 1.43 | 0.06 | 0.35 | 0.42 |

$r_s=10$ there is a very unusual situation in which low-momentum states have a lower occupation than ones near the Fermi surface. There is still a rapid falloff of the momentum distribution at the Fermi surface, but the discontinuity is probably only 20% of its free value. It will be interesting to examine what the momentum distribution looks like with more exact calculational methods in which nodes can change from the Hartree-Fock form.

## ACKNOWLEDGMENTS

Part of this research was performed at the Aspen Center for Physics (Aspen, CO). Both D.M.C. and B.T. are supported by the National Center for Supercomputing Applications (NCSA) and by the Department of Physics at the University of Illinois at Urbana-Champaign. The calculations were performed on the Cray X-MP/48 at the NCSA, which is supported by the U.S. National Science Foundation. We acknowledge useful discussions with Dr. F. Green and Professor D. Pines.

[1]A. J. Dahm and W. F. Vinen, Phys. Today **40**(2),43 (1988).
[2]H. L. Stormer, Surf. Sci. **132**, 519 (1983); Adv. Solid State Phys. **24**, 25 (1981); T. Ando, A. Fowler, and F. Stern, Rev. Mod. Phys. **54**, 437 (1982).
[3]M. Jonson, J. Phys. C **9**, 3055 (1976).
[4]A. K. Rajagopal and J. C. Kimball, Phys. Rev. B **15**, 2819 (1977).
[5]A. Isihara and T. Toyoda, Z. Phys. B **29**, 70 (1978).
[6]D. Ceperley, Phys. Rev. B **18**, 3126 (1978).
[7]D. L. Freeman, Solid State Commun. **26**, 289 (1978).
[8]D. Ceperley and B. J. Alder, Phys. Rev. Lett. **45**, 566 (1980).
[9]L. C. Ioriatti, Jr. and A. Isihara, Z. Phys. B **44**, 1 (1981).
[10]D. L. Freeman, J. Phys. C **16**, 711 (1983).
[11]S. Nagano, K. S. Singwi, and S. Ohnishi, Phys. Rev. B **29**, 1209 (1984).
[12]H. K. Sim, R. Tao, and F. Y. Wu, Phys. Rev. B **34**, 7123 (1986).
[13]M. Imada and M. Takahashi, J. Phys. Soc. Jpn. **53**, 3770 (1984).
[14]N. Metropolis, A. Rosenbluth, M. Rosenbluth, A. H. Teller, and E. Teller, J. Chem. Phys. **21**, 1087 (1953).
[15]P. J. Reynolds, D. M. Ceperley, B. J. Alder, and W. A. Lester, Jr., J. Chem. Phys. **77**, 5593 (1982).
[16]W. L. McMillan, Phys. Rev. **138**, A442 (1965).
[17]D. M. Ceperley, G. V. Chester, and M. H. Kalos, Phys. Rev. B **16**, 3081 (1977).
[18]B. J. Alder, D. M. Ceperley, and P. J. Reynolds, J. Phys. Chem. **86**, 1200 (1982).
[19]T. Gaskell, Proc. Phys. Soc. London **77**, 1182 (1961); **77**, 1791 (1962).
[20]L. D. Landau and E. M. Lifshitz, *Statistical Physics,* 2nd ed. (Addison-Wesley, Reading, MA, 1970), p. 194.

[21]L. Bonsall and A. A. Maradudin, Phys. Rev. B **15**, 1959 (1977).
[22]D. M. Ceperley and G. Jacucci, Phys. Rev. Lett. **58**, 1648 (1987).
[23]M. Roger, Phys. Rev. B **30**, 6432 (1984).
[24]D. M. Ceperley and B. J. Alder, in *Monte Carlo Methods in Statistical Physics,* edited by K. Binder (Springer-Verlag, Berlin, 1979).